

J. S. Yu^{25,h}, T. Yu⁷², X. D. Yu^{46,g}, C. Z. Yuan^{1,63}, L. Yuan², S. C. Yuan¹, Y. Yuan^{1,63}, Z. Y. Yuan⁵⁹, C. X. Yue³⁹, A. A. Zafar⁷³, F. R. Zeng⁵⁰, S. H. Zeng⁷², X. Zeng^{12,f}, Y. Zeng^{25,h}, Y. J. Zeng^{1,63}, X. Y. Zhai³⁴, Y. C. Zhai⁵⁰, Y. H. Zhan⁵⁹, A. Q. Zhang^{1,63}, B. L. Zhang^{1,63}, B. X. Zhang¹, D. H. Zhang⁴³, G. Y. Zhang¹⁹, H. Zhang⁷¹, H. C. Zhang^{1,58,63}, H. H. Zhang⁵⁹, H. H. Zhang³⁴, H. Q. Zhang^{1,58,63}, H. Y. Zhang^{1,58}, J. Zhang⁸⁰, J. Zhang⁵⁹, J. J. Zhang⁵², J. L. Zhang²⁰, J. Q. Zhang⁴¹, J. W. Zhang^{1,58,63}, J. X. Zhang^{38,j,k}, J. Y. Zhang¹, J. Z. Zhang^{1,63}, Jianyu Zhang⁶³, L. M. Zhang⁶¹, L. Q. Zhang⁵⁹, Lei Zhang⁴², P. Zhang^{1,63}, Q. Y. Zhang^{39,80}, Shuihan Zhang^{1,63}, Shulei Zhang^{25,h}, X. D. Zhang⁴⁵, X. M. Zhang¹, X. Y. Zhang⁵⁰, Y. Zhang⁶⁹, Y. Zhang⁷², Y. T. Zhang⁸⁰, Y. H. Zhang^{1,58}, Yan Zhang^{71,58}, Yao Zhang¹, Z. D. Zhang¹, Z. H. Zhang¹, Z. L. Zhang³⁴, Z. Y. Zhang⁴³, Z. Y. Zhang⁷⁶, G. Zhao¹, J. Y. Zhao^{1,63}, J. Z. Zhao^{1,58}, Lei Zhao^{71,58}, Ling Zhao¹, M. G. Zhao⁴³, R. P. Zhao⁶³, S. J. Zhao⁸⁰, Y. B. Zhao^{1,58}, Y. X. Zhao^{31,63}, Z. G. Zhao^{71,58}, A. Zhemchugov^{36,a}, B. Zheng⁷², J. P. Zheng^{1,58}, W. J. Zheng^{1,63}, Y. H. Zheng⁶³, B. Zhong⁴¹, X. Zhong⁵⁹, H. Zhou⁵⁰, L. P. Zhou^{1,63}, X. Zhou⁷⁶, X. K. Zhou⁶, X. R. Zhou^{71,58}, X. Y. Zhou³⁹, Y. Z. Zhou^{12,f}, J. Zhu⁴³, K. Zhu¹, K. J. Zhu^{1,58,63}, L. Zhu³⁴, L. X. Zhu⁶³, S. H. Zhu⁷⁰, S. Q. Zhu⁴², T. J. Zhu^{12,f}, W. J. Zhu^{12,f}, Y. C. Zhu^{71,58}, Z. A. Zhu^{1,63}, J. H. Zou¹, J. Zu^{71,58}

(BESIII Collaboration)

¹ Institute of High Energy Physics, Beijing 100049, People's Republic of China

² Beihang University, Beijing 100191, People's Republic of China

³ Bochum Ruhr-University, D-44780 Bochum, Germany

⁴ Budker Institute of Nuclear Physics SB RAS (BINP), Novosibirsk 630090, Russia

⁵ Carnegie Mellon University, Pittsburgh, Pennsylvania 15213, USA

⁶ Central China Normal University, Wuhan 430079, People's Republic of China

⁷ Central South University, Changsha 410083, People's Republic of China

⁸ China Center of Advanced Science and Technology, Beijing 100190, People's Republic of China

⁹ China University of Geosciences, Wuhan 430074, People's Republic of China

¹⁰ Chung-Ang University, Seoul, 06974, Republic of Korea

¹¹ COMSATS University Islamabad, Lahore Campus, Defence Road, Off Raiwind Road, 54000 Lahore, Pakistan

¹² Fudan University, Shanghai 200433, People's Republic of China

¹³ GSI Helmholtzcentre for Heavy Ion Research GmbH, D-64291 Darmstadt, Germany

¹⁴ Guangxi Normal University, Guilin 541004, People's Republic of China

¹⁵ Guangxi University, Nanning 530004, People's Republic of China

¹⁶ Hangzhou Normal University, Hangzhou 310036, People's Republic of China

¹⁷ Hebei University, Baoding 071002, People's Republic of China

¹⁸ Helmholtz Institute Mainz, Staudinger Weg 18, D-55099 Mainz, Germany

¹⁹ Henan Normal University, Xinxiang 453007, People's Republic of China

²⁰ Henan University, Kaifeng 475004, People's Republic of China

²¹ Henan University of Science and Technology, Luoyang 471003, People's Republic of China

²² Henan University of Technology, Zhengzhou 450001, People's Republic of China

²³ Huangshan College, Huangshan 245000, People's Republic of China

²⁴ Hunan Normal University, Changsha 410081, People's Republic of China

²⁵ Hunan University, Changsha 410082, People's Republic of China

²⁶ Indian Institute of Technology Madras, Chennai 600036, India

²⁷ Indiana University, Bloomington, Indiana 47405, USA

²⁸ INFN Laboratori Nazionali di Frascati , (A)INFN Laboratori Nazionali di Frascati, I-00044, Frascati, Italy; (B)INFN

Sezione di Perugia, I-06100, Perugia, Italy; (C)University of Perugia, I-06100, Perugia, Italy

²⁹ INFN Sezione di Ferrara, (A)INFN Sezione di Ferrara, I-44122, Ferrara, Italy; (B)University of Ferrara, I-44122, Ferrara, Italy

³⁰ Inner Mongolia University, Hohhot 010021, People's Republic of China

³¹ Institute of Modern Physics, Lanzhou 730000, People's Republic of China

³² Institute of Physics and Technology, Peace Avenue 54B, Ulaanbaatar 13330, Mongolia

³³ Instituto de Alta Investigación, Universidad de Tarapacá, Casilla 7D, Arica 1000000, Chile

³⁴ Jilin University, Changchun 130012, People's Republic of China

³⁵ Johannes Gutenberg University of Mainz, Johann-Joachim-Becher-Weg 45, D-55099 Mainz, Germany

³⁶ Joint Institute for Nuclear Research, 141980 Dubna, Moscow region, Russia

³⁷ Justus-Liebig-Universitaet Giessen, II. Physikalisches Institut, Heinrich-Buff-Ring 16, D-35392 Giessen, Germany

³⁸ Lanzhou University, Lanzhou 730000, People's Republic of China

³⁹ Liaoning Normal University, Dalian 116029, People's Republic of China

⁴⁰ Liaoning University, Shenyang 110036, People's Republic of China

⁴¹ Nanjing Normal University, Nanjing 210023, People's Republic of China

⁴² Nanjing University, Nanjing 210093, People's Republic of China

⁴³ Nankai University, Tianjin 300071, People's Republic of China

⁴⁴ National Centre for Nuclear Research, Warsaw 02-093, Poland

⁴⁵ North China Electric Power University, Beijing 102206, People's Republic of China

⁴⁶ Peking University, Beijing 100871, People's Republic of China

⁴⁷ Qufu Normal University, Qufu 273165, People's Republic of China

- ⁴⁸ Renmin University of China, Beijing 100872, People's Republic of China
⁴⁹ Shandong Normal University, Jinan 250014, People's Republic of China
⁵⁰ Shandong University, Jinan 250100, People's Republic of China
⁵¹ Shanghai Jiao Tong University, Shanghai 200240, People's Republic of China
⁵² Shanxi Normal University, Linfen 041004, People's Republic of China
⁵³ Shanxi University, Taiyuan 030006, People's Republic of China
⁵⁴ Sichuan University, Chengdu 610064, People's Republic of China
⁵⁵ Soochow University, Suzhou 215006, People's Republic of China
⁵⁶ South China Normal University, Guangzhou 510006, People's Republic of China
⁵⁷ Southeast University, Nanjing 211100, People's Republic of China
⁵⁸ State Key Laboratory of Particle Detection and Electronics, Beijing 100049, Hefei 230026, People's Republic of China
⁵⁹ Sun Yat-Sen University, Guangzhou 510275, People's Republic of China
⁶⁰ Suranaree University of Technology, University Avenue 111, Nakhon Ratchasima 30000, Thailand
⁶¹ Tsinghua University, Beijing 100084, People's Republic of China
⁶² Turkish Accelerator Center Particle Factory Group, (A)Istinye University, 34010, Istanbul, Turkey; (B)Near East University, Nicosia, North Cyprus, 99138, Mersin 10, Turkey
⁶³ University of Chinese Academy of Sciences, Beijing 100049, People's Republic of China
⁶⁴ University of Groningen, NL-9747 AA Groningen, The Netherlands
⁶⁵ University of Hawaii, Honolulu, Hawaii 96822, USA
⁶⁶ University of Jinan, Jinan 250022, People's Republic of China
⁶⁷ University of Manchester, Oxford Road, Manchester, M13 9PL, United Kingdom
⁶⁸ University of Muenster, Wilhelm-Klemm-Strasse 9, 48149 Muenster, Germany
⁶⁹ University of Oxford, Keble Road, Oxford OX13RH, United Kingdom
⁷⁰ University of Science and Technology Liaoning, Anshan 114051, People's Republic of China
⁷¹ University of Science and Technology of China, Hefei 230026, People's Republic of China
⁷² University of South China, Hengyang 421001, People's Republic of China
⁷³ University of the Punjab, Lahore-54590, Pakistan
⁷⁴ University of Turin and INFN, (A)University of Turin, I-10125, Turin, Italy; (B)University of Eastern Piedmont, I-15121, Alessandria, Italy; (C)INFN, I-10125, Turin, Italy
⁷⁵ Uppsala University, Box 516, SE-75120 Uppsala, Sweden
⁷⁶ Wuhan University, Wuhan 430072, People's Republic of China
⁷⁷ Yantai University, Yantai 264005, People's Republic of China
⁷⁸ Yunnan University, Kunming 650500, People's Republic of China
⁷⁹ Zhejiang University, Hangzhou 310027, People's Republic of China
⁸⁰ Zhengzhou University, Zhengzhou 450001, People's Republic of China
- ^a Also at the Moscow Institute of Physics and Technology, Moscow 141700, Russia
^b Also at the Novosibirsk State University, Novosibirsk, 630090, Russia
^c Also at the NRC "Kurchatov Institute", PNPI, 188300, Gatchina, Russia
^d Also at Goethe University Frankfurt, 60323 Frankfurt am Main, Germany
^e Also at Key Laboratory for Particle Physics, Astrophysics and Cosmology, Ministry of Education; Shanghai Key Laboratory for Particle Physics and Cosmology; Institute of Nuclear and Particle Physics, Shanghai 200240, People's Republic of China
^f Also at Key Laboratory of Nuclear Physics and Ion-beam Application (MOE) and Institute of Modern Physics, Fudan University, Shanghai 200443, People's Republic of China
^g Also at State Key Laboratory of Nuclear Physics and Technology, Peking University, Beijing 100871, People's Republic of China
^h Also at School of Physics and Electronics, Hunan University, Changsha 410082, China
ⁱ Also at Guangdong Provincial Key Laboratory of Nuclear Science, Institute of Quantum Matter, South China Normal University, Guangzhou 510006, China
^j Also at MOE Frontiers Science Center for Rare Isotopes, Lanzhou University, Lanzhou 730000, People's Republic of China
^k Also at Lanzhou Center for Theoretical Physics, Lanzhou University, Lanzhou 730000, People's Republic of China
^l Also at the Department of Mathematical Sciences, IBA, Karachi 75270, Pakistan

We search for the di-photon decay of a light pseudoscalar axion-like particle, a , in radiative decays of the J/ψ , using 10 billion J/ψ events collected with the BESIII detector. We find no evidence of a narrow resonance and set upper limits at the 95% confidence level on the product branching fraction $\mathcal{B}(J/\psi \rightarrow \gamma a) \times \mathcal{B}(a \rightarrow \gamma\gamma)$ and the axion-like particle photon coupling constant $g_{a\gamma\gamma}$ in the ranges of $(3.6 - 49.8) \times 10^{-8}$ and $(2.2 - 103.8) \times 10^{-4} \text{ GeV}^{-1}$, respectively, for $0.18 \leq m_a \leq 2.85 \text{ GeV}/c^2$. These are the most stringent limits to date in this mass region.

Axions are hypothetical pseudoscalar gauge bosons originally proposed by Peccei and Quinn as a mechanism of spontaneous breaking of $U(1)$ symmetry to re-

solve the strong CP problem in quantum chromodynamics [1–3] and later applied to the electroweak hierarchy problem [4]. Axion-like particles (ALPs) appear in vari-

ous extensions of the Standard Model (SM), such as supersymmetry [5–7], extended Higgs sector [8], and string theory [9–12]. Their couplings provide a portal between the dark-sector and SM particles [13] and they could be cold dark matter candidates in certain situations [14–17]. They could also be a graviton-like spin-2 particle [18], CP -violating MSSM [19] or Fermi-phobic Higgs bosons [20]. Experimental constraints on these scenarios are important to understand the properties of the SM Higgs boson [21].

The ALPs have the same quantum numbers as the QCD axion, but they have different masses and couplings. In a simple scenario, the ALP, a , predominantly couples to a photon pair with a coupling constant $g_{a\gamma\gamma}$. Experimental bounds on $g_{a\gamma\gamma}$ for masses of a in the sub-MeV/ c^2 range are available from laser experiments, solar photon instruments and astrophysical observations [22, 23], while the experimental bounds on the photon coupling in the MeV/ c^2 –GeV/ c^2 range mainly come from beam-dump and high-energy collider experiments [24–26].

Limits on long-lived ALPs are derived from radiative decays $V \rightarrow \gamma + \text{invisible}$ ($V = \Upsilon(1S), J/\psi$) [27, 28] and the $e^+e^- \rightarrow \gamma + \text{invisible}$ reactions [29], which is a reinterpretation of BaBar measurements [30–32]. On the other hand, short-lived ALPs decaying to a photon pair are searched for in $e^+e^- \rightarrow \gamma\gamma(\gamma)$ reactions [33–35], the light-by-light scattering process $\gamma\gamma \rightarrow \gamma\gamma$ [36, 37], pp collisions [38–40] and radiative $J/\psi \rightarrow \gamma a$ decays, based on 2.7 billion $\psi(3686)$ events at BESIII [41]. The ALP-photon coupling in the ALP mass range of (0.1–10) GeV/ c^2 is less constrained compared to the other mass regions. The large data sample collected by the BESIII detector at the J/ψ resonance [42] can further improve the sensitivity on $g_{a\gamma\gamma}$ in the ALP mass region of $0.18 \leq m_a \leq 2.85$ GeV/ c^2 [43].

In J/ψ decays, ALP production predominantly proceeds via the radiative decay $J/\psi \rightarrow \gamma a$ [44]. The branching fraction of $J/\psi \rightarrow \gamma a$ relates to $g_{a\gamma\gamma}$ as [44]

$$\frac{\mathcal{B}(J/\psi \rightarrow \gamma a)}{\mathcal{B}(J/\psi \rightarrow e^+e^-)} = \frac{m_{J/\psi}^2}{32\pi\alpha} g_{a\gamma\gamma}^2 \left(1 - \frac{m_a^2}{m_{J/\psi}^2}\right)^3, \quad (1)$$

where α is the fine-structure constant, m_a is the mass of the ALP and $m_{J/\psi}$ is the mass of the J/ψ meson. Additional processes contributing to the same final state are ALP production from the ALP-strahlung $e^+e^- \rightarrow \gamma a$ process [44] and the radiative production of pseudoscalar mesons through $J/\psi \rightarrow \gamma P$ with $P = \{\pi^0, \eta, \eta', \eta_c\}$ [45, 46].

This paper describes the search for a light pseudoscalar ALP particle in radiative decays of the J/ψ using $(1.0087 \pm 0.0044) \times 10^{10}$ J/ψ events collected with the BESIII detector [42]. This search assumes that the direct coupling of the ALP to charm quarks is negligible, and that the ALP produced in $J/\psi \rightarrow \gamma a$ couples to the virtual photon created in $c\bar{c}$ annihilation [44]. Because it is impossible to make a distinction between the

ALP-strahlung process $e^+e^- \rightarrow \gamma a$ and radiative decay $J/\psi \rightarrow \gamma a$, in the case of a null result, the expected 4.4% pollution from the ALP-strahlung $e^+e^- \rightarrow \gamma a$ process [44] in J/ψ data will be considered as a systematic uncertainty in this search. The interference between the ALP-strahlung process $e^+e^- \rightarrow \gamma a$ and radiative $J/\psi \rightarrow \gamma a$ is predicted to be negligible due to the small J/ψ width [44].

The BESIII detector [47] records symmetric e^+e^- collisions provided by the BEPCII storage ring [48] in the center-of-mass energy range from 2.0 to 4.95 GeV with a peak luminosity of 1×10^{33} cm $^{-2}$ s $^{-1}$ achieved at $\sqrt{s} = 3.77$ GeV. BESIII has collected large data samples in this energy region [49]. The cylindrical core of the BESIII detector covers 93% of the full solid angle and consists of a helium-based multi-layer drift chamber (MDC), a plastic scintillator time-of-flight system (TOF), and a CsI(Tl) electromagnetic calorimeter (EMC), which are all enclosed in a superconducting solenoidal magnet providing a 1.0 T (0.9 T in 2012, for about 11% of the dataset) magnetic field. The solenoid is supported by an octagonal flux-return yoke with resistive plate counter muon identification modules interleaved with steel. The charged-particle momentum resolution at 1 GeV/ c is 0.5%. The EMC measures photon energies with a resolution of 2.5% (5%) at 1 GeV in the barrel (end cap) region. The time resolution in the TOF barrel region is 68 ps, while that in the end cap region is 110 ps. The end cap TOF system was upgraded in 2015 using multigap resistive plate chamber technology, providing a time resolution of 60 ps. About 87% of the dataset benefits from this upgrade.

Monte Carlo (MC) simulated data samples produced with a GEANT4-based software package [50], which includes the geometrical acceptance of the detector and time-dependent beam related backgrounds, are used to optimize the event selection criteria, study the potential backgrounds and evaluate the reconstruction efficiency. An MC sample of 10 billion inclusive J/ψ events is used for background studies with the TopoAna tool [51]. In this sample, the known decay modes of J/ψ are simulated by EVTGEN [52] with their branching fractions taken from the Particle Data Group (PDG) [45] and the remaining unknown decay modes by LUNDCHARM [53]. The production of the J/ψ resonance via e^+e^- annihilation, including beam energy spread and initial-state radiation (ISR), is simulated by KKMC [54]. The backgrounds from the SM processes $e^+e^- \rightarrow \gamma\gamma(\gamma)$ and $e^+e^- \rightarrow \gamma P$ (here P is a pseudoscalar meson) are estimated with 166.3 pb $^{-1}$ of continuum data collected at the center-of-mass energy of 3.08 GeV [42]. To evaluate the signal efficiency, simulated signal MC events are generated for 33 values of m_a ranging from 0.1 GeV/ c^2 to 3.0 GeV/ c^2 with a phase-space model for $a \rightarrow \gamma\gamma$ and a P -wave model for the $J/\psi \rightarrow \gamma a$ decay [52].

We select the events of interest with at least three photon candidates and zero charged tracks in the final state. The photon candidates are reconstructed using the energy clusters deposited in the EMC barrel region with a

minimum energy of 25 MeV. Endcap clusters are not used in order to suppress the background from $e^+e^- \rightarrow \gamma\gamma(\gamma)$ events. The energy deposited in the nearby TOF scintillators is also included to improve the reconstruction efficiency and energy resolution. The EMC time difference between any two photons is required to be within the range of $-500 < \Delta T < 500$ ns to suppress electronic noise and energy deposits unrelated to the events. To improve the mass resolution, the invariant mass of the three final state photons is forced to the J/ψ nominal mass using a four-constraint (4C) kinematic fit. If there is more than one $J/\psi \rightarrow \gamma\gamma\gamma$ combination, the candidate with the minimum value of the χ^2 from the kinematic fit (χ^2_{4C}) is retained. A similar 4C kinematic fit is also separately performed with all possible two, four and five photon candidate hypotheses. We require that the χ^2_{4C} of the three photon candidate hypothesis is less than that for the other hypotheses. The χ^2_{4C} of three photon candidates is further required to be less than 30 to suppress background contributions from $e^+e^- \rightarrow \gamma\gamma$ and $J/\psi \rightarrow \gamma\pi^0\pi^0$ decays. The selected three photon candidates are used for further analysis.

In order to further suppress the $e^+e^- \rightarrow \gamma\gamma(\gamma)$ events with low-energy EMC clusters, the energy difference between the first (second) and third photon candidates, $\Delta E_{\gamma_{ij}}$, is required to be less than 1.46 (1.41) GeV, where the first, second and third photons are sorted by decreasing energy. The absolute azimuthal angle difference between the third and first photon candidates, $\Delta\phi_{\gamma_{31}}$, is also required to be greater than 1 radian.

At this stage, the dominant background contributions mainly come from $J/\psi \rightarrow \gamma P$, where P denotes the pseudoscalar mesons $\pi^0, \eta, \eta', \eta_c$, as also seen in Refs. [41, 46]. To validate the fit procedure to determine the signal yield (see below), the same procedure is used to extract the branching fractions of $J/\psi \rightarrow \gamma(\pi^0, \eta, \eta') \rightarrow \gamma\gamma\gamma$. After accounting for the peaking background contributions, the results are compatible with the measurements of Ref. [46] within the uncertainties. In the further analysis we reject the events where the di-photon invariant mass ($m_{\gamma\gamma}$) for any photon combination is in the regions $0.11 \leq m_{\gamma\gamma} \leq 0.16$ GeV/ c^2 , $0.52 \leq m_{\gamma\gamma} \leq 0.56$ GeV/ c^2 , $0.92 \leq m_{\gamma\gamma} \leq 0.99$ GeV/ c^2 , and $2.92 \leq m_{\gamma\gamma} \leq 3.04$ GeV/ c^2 to suppress the backgrounds from $J/\psi \rightarrow \gamma\pi^0$, $J/\psi \rightarrow \gamma\eta$, $J/\psi \rightarrow \gamma\eta'$ and $J/\psi \rightarrow \gamma\eta_c$, respectively.

After applying the above selection criteria, the signal yields are extracted from data by performing a series of one-dimensional unbinned extended maximum likelihood (ML) fit to the $m_{\gamma\gamma}$ distribution, which includes all three photon pair combinations. The fit function includes the contributions of signal and backgrounds and is described in more detail below. Fig. 1 shows the $m_{\gamma\gamma}$ distribution for data and various background predictions. The dominant background comes from the QED process $e^+e^- \rightarrow \gamma\gamma(\gamma)$, which is predicted from the continuum data collected at 3.08 GeV. The $m_{\gamma\gamma}$ distribution of data is generally well-described by the background predictions, except in the low-mass region, where KKMC [54]

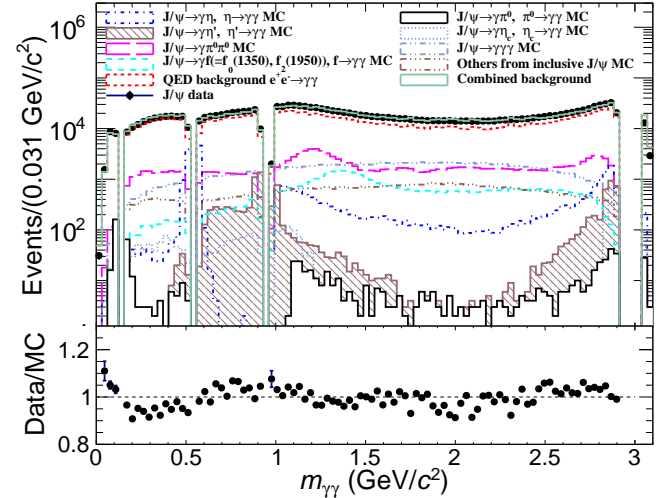


FIG. 1. Distribution of $m_{\gamma\gamma}$ in data (black dots with error bars) together with the background predictions of the QED $e^+e^- \rightarrow \gamma\gamma$ process from data collected at 3.08 GeV (dashed red curve), $J/\psi \rightarrow \gamma\pi^0\pi^0$ (long-dashed pink curve), $J/\psi \rightarrow \gamma\gamma\gamma$ (double-dotted long-dashed grey curve), $J/\psi \rightarrow \gamma f$ ($f = f_0(1350), f_2(1950)$) (long-dashed cyan curve), $J/\psi \rightarrow \gamma P$ (brown pattern, dashed-dotted blue, black and dotted grey histograms) and other backgrounds from inclusive J/ψ decays (triple dotted long-dashed brown curve). The solid green olive histogram represents the combined background. The bottom figure shows the ratio of data to the combined background predictions.

TABLE I. The fit intervals of $m_{\gamma\gamma}$ for various m_a points.

m_a range (GeV/ c^2)	$m_{\gamma\gamma}$ fit interval (GeV/ c^2)	Polynomial function order
0.180 – 0.420	0.16, 0.46	4 th
0.421 – 0.490	0.39, 0.51	5 th
0.610 – 0.880	0.59, 0.90	5 th
1.020 – 1.099	1.00, 1.20	5 th
1.100 – 2.770	$m_a - 0.10, m_a + 0.10$	3 rd
2.772 – 2.850	2.70, 2.88	4 th

fails to reproduce the events for J/ψ decaying to multi-photons in the final state. This disagreement has a minor impact on the ALP search because the signal event extraction procedure does not depend on the predictions of the background yields. In order to mitigate the effect from the tails of the peaking backgrounds $J/\psi \rightarrow \gamma P$, the fit is performed in different $m_{\gamma\gamma}$ intervals for various m_a points, as described in Table I.

Simulated data samples are used to construct the signal and non-peaking background probability density distribution functions (PDFs). The signal PDF is described by the sum of two Crystal Ball functions with common mean and opposite-side tails. The efficiency and parameters of the Crystal Ball functions are obtained from the simulated signal MC samples by performing a fit to the $m_{\gamma\gamma}$ distribution. This fit includes the contribu-

tions of signal and combinatorial background from wrong $\gamma\gamma$ combinations, described by a first-order Chebyshev function. The m_a resolution varies from 6 MeV/ c^2 to 15 MeV/ c^2 while the signal selection efficiency, ϵ , varies from 28.2% to 39.0% depending on the a mass. The PDF parameters and efficiency of the signal are interpolated linearly between the mass points of the generated signal MC samples. The non-peaking background PDF is described by 3rd-, 4th- and 5th-order Chebyshev functions in various $m_{\gamma\gamma}$ fit regions detailed in Table I.

The search for a narrow a resonance is performed in 1.0 MeV/ c^2 steps in the mass range of $0.18 \leq m_a \leq 1.5$ GeV/ c^2 and 2.0 MeV/ c^2 steps for higher m_a values. The free parameters of the fit are the number of signal events (N_{sig}), the number of background events and the shape parameters of the non-peaking background PDF. To take into account a possible systematic uncertainty associated with the choice of PDFs, the fit is repeated with an alternative signal PDF described by a Cruijff function [55] and increasing by one the order of the Chebyshev polynomial function for the non-peaking background PDF at each m_a point. The fit with the largest signal yield, giving the worst upper limit, is chosen to produce the final result. We calculate the product branching fraction of $J/\psi \rightarrow \gamma a$ and $a \rightarrow \gamma\gamma$ at each m_a point using the following formula,

$$\mathcal{B}(J/\psi \rightarrow \gamma a) \times \mathcal{B}(a \rightarrow \gamma\gamma) = \frac{N_{\text{sig}}}{\epsilon N_{J/\psi}}. \quad (2)$$

Figure 2 shows the product branching fraction $\mathcal{B}(J/\psi \rightarrow \gamma a) \times \mathcal{B}(a \rightarrow \gamma\gamma)$ and the statistical significance, defined as $\mathcal{S} = \sqrt{-2\ln(\mathcal{L}_0/\mathcal{L}_{\text{max}})}$, as a function of m_a , where \mathcal{L}_{max} and \mathcal{L}_0 are the likelihood functions for the number of signal events obtained from the fit and fixed at zero, respectively. The largest value of upward local significance is determined to be 3.5σ at $m_a = 2.786$ GeV/ c^2 . The fit result for the corresponding m_a point is shown in Fig. 3. We estimate the probability of observing a fluctuation of $\mathcal{S} \geq 3.5\sigma$ to be 5.2% using a large ensemble of pseudo-experiments [56]. The corresponding global significance value is 1.6σ . Thus, we conclude that no significant evidence of signal events is found within the investigated m_a regions.

As follows from Eqs. 1 and 2, the systematic uncertainties for the coupling of the ALP to a photon pair and the branching fraction measurements include those from the number of signal events, the reconstruction efficiency, the total number of J/ψ events, the branching fraction of $J/\psi \rightarrow e^+e^-$ and expected 4.4% pollution from ALP-strahlung $e^+e^- \rightarrow \gamma a$ process [44]. The uncertainties associated with the number of signal events are additive because they originate from the PDF parameters of signal and backgrounds and the fit bias. The additive systematic uncertainty affects the significance of any observations and does not scale with the number of reconstructed signal events. We take into account the uncertainties associated with the PDF parameters of signal

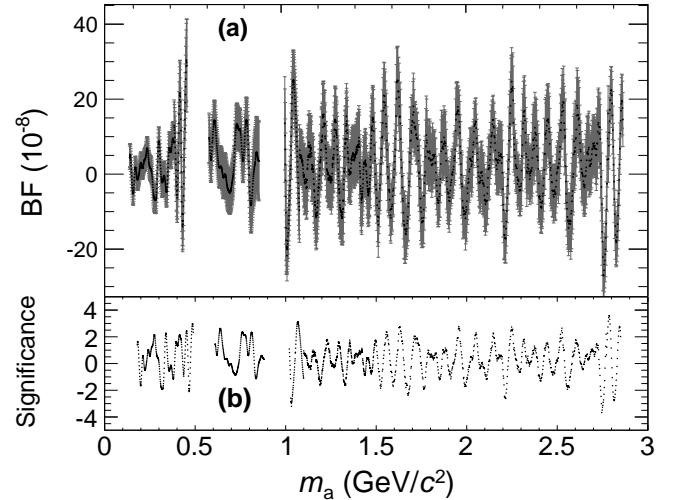


FIG. 2. (a) Product branching fraction $\mathcal{B}(J/\psi \rightarrow \gamma a) \times \mathcal{B}(a \rightarrow \gamma\gamma)$ (BF) and (b) the signal significance (\mathcal{S}) versus m_a obtained from the fit, as described above.

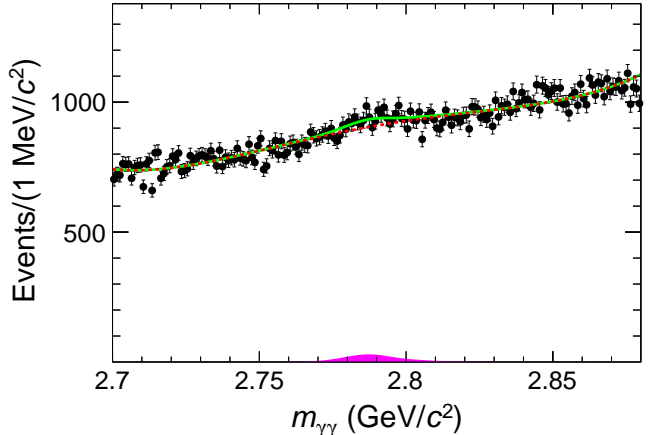


FIG. 3. Fit to the $m_{\gamma\gamma}$ distribution for $m_a = 2.786$ GeV/ c^2 . The black dots with error bars represent data, the dashed pink curve is the continuum background, the filled pink curve is the signal PDF and the solid green curve is the total fit result.

and non-peaking backgrounds by performing the alternative fits at each m_a point using alternative PDFs, as described above. We utilize a large number of pseudo-experiments to test the reliability of the ML fit procedure and the accuracy of the signal and background modeling. The signal yields are extracted from these toy data using the same fit method described above. The biases are consistent with zero and their average uncertainty is 9.2 events, which is taken as an additional additive systematic uncertainty (σ_{add}).

The other sources of the systematic uncertainties are multiplicative; they scale with the number of reconstructed events and do not affect the significance of a yield. The uncertainty associated with the reconstruc-

tion efficiency includes contributions from the 4C kinematic fit, the selection criteria of ΔE_{ij} and $\Delta\phi_{13}$ and photon detection efficiency.

We use a control sample of $J/\psi \rightarrow \gamma\eta$, $\eta \rightarrow \gamma\gamma$ to evaluate the systematic uncertainties associated with the χ^2_{4C} , $\Delta E_{\gamma_{13}}$, $\Delta E_{\gamma_{23}}$, $J/\psi \rightarrow \gamma P$ veto, and $\Delta\phi_{13}$ requirements. The signal yields for $J/\psi \rightarrow \gamma\eta$ from both data and MC simulation are extracted by performing an ML fit to the $m_{\gamma\gamma}$ distribution using the same fit procedure as described above. The corresponding systematic uncertainties, computed as the relative change in efficiency between data and MC simulation, are determined to be 2.3%, 0.1%, 0.1%, 0.8% and 0.1%, respectively. The systematic uncertainty associated with the total number of J/ψ events is determined to be 0.44% with a sample of inclusive J/ψ hadronic events [42].

A control sample of $e^+e^- \rightarrow \gamma\mu^+\mu^-$ is used to evaluate the systematic uncertainty associated with the photon reconstruction efficiency. An ISR photon in this control sample is predicted using the four momenta of the two charged particles. This sample also includes the contributions from $e^+e^- \rightarrow \gamma\pi^+\pi^-$ and $J/\psi \rightarrow \gamma\pi^+\pi^-$, including all the possible intermediate resonances. The relative difference of efficiency between data and MC simulation is determined to be 0.2% per photon [57]. Thus, the total systematic uncertainty due to photon reconstruction efficiency for three photon candidates is 0.6%. The uncertainty associated with the branching fraction of $J/\psi \rightarrow e^+e^-$ is 0.5% taken from the PDG [45]. The total multiplicative systematic uncertainty (σ_{mult}) is obtained by adding the individual ones in quadrature, and is determined to be 2.6% and 5.1% for the product branching fraction $\mathcal{B}(J/\psi \rightarrow \gamma a) \times \mathcal{B}(a \rightarrow \gamma\gamma)$ and coupling of ALP to a photon pair $g_{a\gamma\gamma}$, respectively. All the sources of the systematic uncertainties are summarized in Table II. We calculate the final systematic uncertainty as $\sqrt{\sigma_{\text{add}}^2 + (\sigma_{\text{mult}} \times N_{\text{sig}})^2}$.

TABLE II. The sources of the systematic uncertainties. The uncertainties associated with the signal and background PDFs are incorporated in the fitting, as described in the text.

Source	Uncertainty	
	$J/\psi \rightarrow \gamma a$	$g_{a\gamma\gamma} (\text{GeV})^{-1}$
Additive (events)		
Fit Bias	9.2	9.2
Multiplicative (%)		
Contamination of $e^+e^- \rightarrow \gamma a$	–	4.4
χ^2_{4C}	2.3	2.3
$\Delta E_{\gamma_{13}}$	0.1	0.1
$\Delta E_{\gamma_{23}}$	0.1	0.1
$J/\psi \rightarrow \gamma P$ veto	0.8	0.8
$\Delta\phi_{\gamma_{31}}$	0.1	0.1
$\mathcal{B}(J/\psi \rightarrow e^+e^-)$	–	0.5
J/ψ counting	0.44	0.44
Photon detection efficiency	0.6	0.6
Total	2.6	5.1

Since no significant evidence of any signal events is

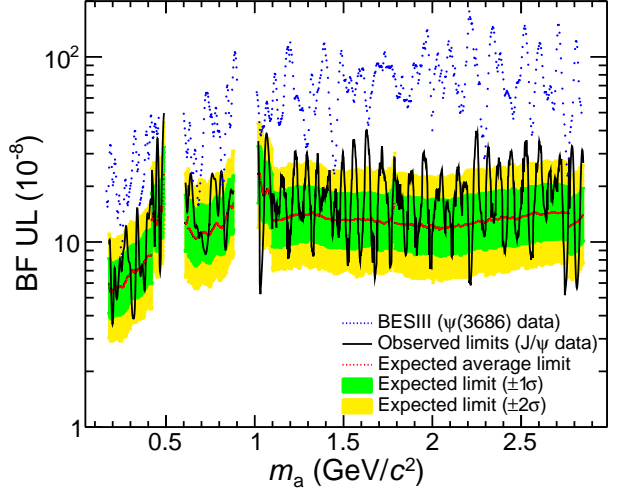


FIG. 4. Upper limits at the 95% C.L. on the product branching fraction $\mathcal{B}(J/\psi \rightarrow \gamma a) \times \mathcal{B}(a \rightarrow \gamma\gamma)$ together with expected limit bands at $\pm 1\sigma$ and $\pm 2\sigma$ levels, obtained from a large ensemble of pseudo-experiments, and compared with the previous BESIII measurements [41] as a function of m_a including the systematic uncertainties. The green and yellow bands of expected limits include the statistical uncertainty only.

found, we set the 95% confidence level (CL) upper limits on the product branching fraction $\mathcal{B}(J/\psi \rightarrow \gamma a) \times \mathcal{B}(a \rightarrow \gamma\gamma)$ as a function of m_a using a Bayesian approach with a uniform prior. The systematic uncertainty is included by convolving the likelihood function with a Gaussian function having a width equal to the systematic uncertainty, as described above. The limits range between $(3.6 - 49.8) \times 10^{-8}$ for $0.18 \leq m_a \leq 2.85 \text{ GeV}/c^2$, as shown in Fig. 4 together with expected limit bands at $\pm 1\sigma$ and $\pm 2\sigma$ levels obtained from a large ensemble of pseudo-experiments. Our result is improved on average by a factor of 8 – 9 over the previous BESIII measurement [41]. Finally, we also calculate the 95% CL upper limit on $g_{a\gamma\gamma}$ using Eq. 1 while assuming $\mathcal{B}(a \rightarrow \gamma\gamma) = 1$ and including the additional sources of the systematic uncertainties on $\mathcal{B}(J/\psi \rightarrow e^+e^-)$ and the expected contribution of the ALP-strahlung $e^+e^- \rightarrow \gamma a$ process [44]. The corresponding exclusion range is shown in Fig. 5. The limit varies within $(2.2 - 103.8) \times 10^{-4} (\text{GeV})^{-1}$ for $0.18 \leq m_a \leq 2.85 \text{ GeV}/c^2$ and is improved by a factor of about 2, 3 and 5, respectively, over the OPAL [33], previous BESIII [41] and Belle II results [35].

In summary, we search for di-photon decays of a light pseudoscalar particle in radiative decays of the J/ψ , using 10 billion J/ψ events collected by the BESIII detector. No significant evidence of signal events is found, and we set 95% CL upper limits on the product branching fraction $\mathcal{B}(J/\psi \rightarrow \gamma a) \times \mathcal{B}(a \rightarrow \gamma\gamma)$ and the coupling of the ALP to a photon pair $g_{a\gamma\gamma}$ as a function of m_a . The corresponding limits are more stringent than the existing limits from OPAL [33], previous BESIII [41] and Belle II [35] results for $0.18 \leq m_a \leq 2.85 \text{ GeV}/c^2$. Thus, our

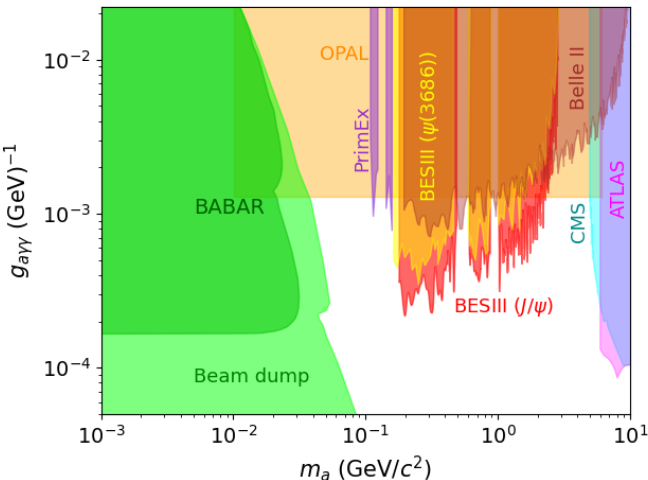


FIG. 5. The 95% CL upper limits on the coupling of ALP to a photon pair ($g_{a\gamma\gamma}$) together with BaBar [29], CMS [36], ATLAS [37], PrimEx [24], beam-dump [25, 26], OPAL [33], previous BESIII [41] and Belle II [35] measurements as a function of m_a , including the systematic uncertainties.

improved limits can significantly constrain the parameter spaces of the extended Higgs sector models [8, 19, 20, 44] and other new physics models [5–7, 13, 18] in the investigated mass region.

Acknowledgement

The BESIII Collaboration thanks the staff of BEPCII and the IHEP computing center for their strong support. This work is supported in part by National Key R&D Program of China under Contracts Nos.

2020YFA0406300, 2020YFA0406400; National Natural Science Foundation of China (NSFC) under Contracts Nos. 11635010, 11735014, 11835012, 11935015, 11935016, 11935018, 11961141012, 12025502, 12035009, 12035013, 12061131003, 12192260, 12192261, 12192262, 12192263, 12192264, 12192265, 12221005, 12225509, 12235017, 11950410506, 11705192; the Chinese Academy of Sciences (CAS) Large-Scale Scientific Facility Program; the CAS Center for Excellence in Particle Physics (CCEPP); Joint Large-Scale Scientific Facility Funds of the NSFC and CAS under Contract No. U1832207; CAS Key Research Program of Frontier Sciences under Contracts Nos. QYZDJ-SSW-SLH003, QYZDJ-SSW-SLH040; 100 Talents Program of CAS; The Institute of Nuclear and Particle Physics (INPAC) and Shanghai Key Laboratory for Particle Physics and Cosmology; European Union’s Horizon 2020 research and innovation programme under Marie Skłodowska-Curie grant agreement under Contract No. 894790; German Research Foundation DFG under Contracts Nos. 455635585, Collaborative Research Center CRC 1044, FOR5327, GRK 2149; Istituto Nazionale di Fisica Nucleare, Italy; Ministry of Development of Turkey under Contract No. DPT2006K-120470; National Research Foundation of Korea under Contract No. NRF-2022R1A2C1092335; National Science and Technology fund of Mongolia; National Science Research and Innovation Fund (NSRF) via the Program Management Unit for Human Resources & Institutional Development, Research and Innovation of Thailand under Contract No. B16F640076; Polish National Science Centre under Contract No. 2019/35/O/ST2/02907; The Swedish Research Council; U. S. Department of Energy under Contract No. DE-FG02-05ER41374

-
- [1] R. D. Peccei and H. R. Quinn, Phys. Rev. Lett. **38**, 1440 (1977); Phys. Rev. D **16**, 1791 (1977).
- [2] S. Weinberg, Phys. Rev. Lett. **40**, 223 (1978).
- [3] F. Wilczek, Phys. Rev. Lett. **40**, 279 (1978).
- [4] P. W. Graham, D. E. Kaplan and S. Rajendran, Phys. Rev. Lett. **115**, 221801 (2015).
- [5] J. Frere, D. Jones and S. Raby, Nucl. Phys. B **222**, 11 (1983).
- [6] A. E. Nelson and N. Seiberg, Nucl. Phys. B **416**, 46 (1994).
- [7] J. Bagger, E. Poppitz and L. Randall, Nucl. Phys. B **426**, 3 (1994).
- [8] G. C. Branco *et al.*, Phys. Rept. **516**, 1 (2012).
- [9] E. Witten, Phys. Lett. B **149**, 351 (1984).
- [10] J. P. Conlon, J. High Energy Phys. **05**, 078 (2006).
- [11] P. Svrcek and E. Witten, J. High Energy Phys. **06**, 051 (2006).
- [12] A. Arvanitaki, S. Dimopoulos, S. Dubovsky, N. Kaloper and J. March-Russell, Phys. Rev. D **81**, 123530 (2010).
- [13] M. Freytsis and Z. Ligeti, Phys. Rev. D **83**, 115009 (2011).
- [14] J. Preskill, M. B. Wise and F. Wilczek, Phys. Lett. B **120**, 127 (1983).
- [15] L. F. Abbott and P. Sikivie, Phys. Lett. B **120**, 133 (1983).
- [16] M. Dine and W. Fischler, Phys. Lett. B **120**, 137 (1983).
- [17] R. A. Battye, B. Garbrecht, J. I. McDonald, F. Pace, and S. Srinivasan, Phys. Rev. D **102**, 023504 (2020).
- [18] D. D. Enterria, M. A. Tamlihat, L. Schoeffel, H. S. Shao and Y. Tayalati, arXiv:2306.15558 (2023).
- [19] S. Hesselbach, S. Moretti, S. Munir and P. Poulose, The Euro. Phys. J. C **54**, 129 (2008).
- [20] A. Delgado, M. G. Pepin, M. Quiros, J. Santiago and R. V. Morales, J. High Energy Phys. **06**, 042 (2016).
- [21] M. Lisanti and J. G. Wacker, Phys. Rev. D **79**, 115006 (2009).
- [22] P. W. Graham *et al.*, Rev. Nucl. Part. Sci. **65**, 485 (2015).
- [23] D. Cadamuro and J. Redondo, JCAP **02**, 032 (2012).
- [24] D. Aloni *et al.*, Phys. Rev. Lett. **123**, 071801 (2019).
- [25] B. Dobrich *et al.*, J. High Energy Phys. **02**, 018 (2016).
- [26] D. Banerjee *et al.* (NA64 Collaboration), Phys. Rev. Lett. **125**, 081801 (2020).
- [27] M. Ablikim *et al.* (BESIII Collaboration), Phys. Rev. D **101**, 112005 (2020).
- [28] I. S. Seong *et al.* (Belle Collaboration), Phys. Rev. Lett. **122**, 011801 (2019).

- [29] M. J. Dolan *et al.*, J. High Energy Phys. **12**, 094 (2017); **03**, 190(E) (2021).
- [30] J. P. Lees *et al.* (BaBar Collaboration), Phys. Rev. Lett. **119**, 131804 (2017).
- [31] B. Aubert *et al.* (BaBar Collaboration), arXiv:0808.0017 (2008).
- [32] P. del Amo Sanchez *et al.* (BaBar Collaboration), Phys. Rev. Lett. **107**, 021804 (2011).
- [33] S. Knapen *et al.*, Phys. Rev. Lett. **118**, 171801 (2017); G. Abbiendi *et al.* (OPAL Collaboration), Eur. Phys. J. C**26**, 331 (2003).
- [34] M. Acciarri *et al.* (L3 Collaboration), Phys. Lett. B **345**, 609 (1995).
- [35] F. Abudinen *et al.* (Belle II Collaboration), Phys. Rev. Lett. **125**, 161806 (2020).
- [36] A. M. Sirunyan *et al.* (CMS Collaboration), Phys. Lett. B **797**, 134826 (2019).
- [37] G. Aad *et al.* (ATLAS Collaboration), J. High Energy Phys. **03**, 243 (2021); **11**, 050(E) (2021).
- [38] D. d'Enterria, Workshop on Feebly Interacting Particles (2021), arXiv:2102.08971.
- [39] G. Aad *et al.* (ATLAS Collaboration), Phys. Rev. Lett. **113**, 171801 (2014).
- [40] G. Aad *et al.* (ATLAS Collaboration), Eur. Phys. J. C **76**, 210 (2016).
- [41] M. Ablikim *et al.* (BESIII Collaboration), Phys. Lett. B **838**, 137698 (2023).
- [42] M. Ablikim *et al.* (BESIII Collaboration), Chin. Phys. C **46**, 074001 (2022).
- [43] J. Jaeckel and M. Spannowsky, Phys. Lett. B **753**, 482 (2016).
- [44] L. Merlo *et al.*, J. High Energy Phys. **06**, 091 (2019).
- [45] R.L. Workman *et al.* (Particle Data Group), Prog. Theor. Exp. Phys. **2022**, 083C01 (2022).
- [46] M. Ablikim *et al.* (BESIII Collaboration), to be published in Phys. Rev. D.
- [47] M. Ablikim *et al.* (BESIII Collaboration), Nucl. Instrum. Methods Phys. Res., Sect. A **614**, 345 (2010); K. X. Huang, *et al.*, Nucl. Sci. Tech. **33**, 142 (2022).
- [48] C. H. Yu *et al.*, Proceedings of IPAC2016, Busan, Korea, 2016, doi:10.18429/JACoW-IPAC2016-TUYA01.
- [49] M. Ablikim *et al.* (BESIII Collaboration), Chin. Phys. C **44**, 040001 (2020).
- [50] S. Agostinelli *et al.* (GEANT4 Collaboration), Nucl. Instrum. Meth. A **506**, 250 (2003).
- [51] X. Y. Zhou, S. X. Du, G. Li and C. P. Shen, Comput. Phys. Commun. **258**, 107540 (2021).
- [52] D. J. Lange, Nucl. Instrum. Method. Phys. Res., Sect. A **462**, 152 (2001); R.G. Ping, Chin. Phys. C **32**, 599 (2008).
- [53] J. C. Chen, G. S. Huang, X. R. Qi, D. H. Zhang and Y. S. Zhu, Phys. Rev. D **62**, 034003 (2000).
- [54] S. Jadach, B. F. L. Ward and Z. Was, Phys. Rev. D **63**, 113009 (2001).
- [55] The Cruijff function is an asymmetric Gaussian function having a common mean (μ), different left-right resolutions ($\sigma_{L,R}$) and non-Gaussian tails ($\alpha_{L,R}$): $f(x) = \exp((x - \mu)^2 / (2\sigma_{L,R}^2 + \alpha_{L,R}(x - \mu)^2))$.
- [56] J. P. Lees *et al.* (BaBar Collaboration), Phys. Rev. D **87**, 059903(R) (2013); V. Prasad, Ph.D. thesis [Report No. SLAC-R-1008, 2013 (unpublished)], arXiv:1307.4560 (2013).
- [57] M. Ablikim *et al.* (BESIII Collaboration), Phys. Rev. D **105**, 012008 (2022).